Activation Energy of Hydrogen Desorption from High-Performance Titanium Oxide Carrier-Selective Contacts with Silicon Oxide Interlayers

Kazuhiro Gotoh[1,], Takeya Mochizuki[1], Tomohiko Hojo[2], Yuki Shibayama[2], Yasuyoshi Kurokawa[1], Eiji Akiyama[2], and Noritaka Usami[1]*

[1]Graduate School of Engineering, Nagoya University, Furo-Cho, Chikusa-ku, Nagoya, Aichi 464-8603, Japan

[2]Institute for Materials Research, Tohoku University, 2-1-1 Katahira, Aoba-ku, Sendai, Miyagi 980-8577, Japan

*Corresponding Author

E-mail: gotoh.kazuhiro@material.nagoya-u.ac.jp

1 Abstract

2 The impact of hydrogen desorption on the electrical properties of TiO_x on crystalline silicon (c-
3 Si) with SiO_y interlayers is studied for the development of high-performance TiO_x carrier-
4 selective contacts. Compared with the TiO_x/c-Si heterocontacts, a lower surface recombination
5 velocity of 9.6 cm/s and lower contact resistivity of 7.1 $m\Omega \cdot cm^2$ are obtained by using SiO_y
6 interlayers formed by mixture (often called SC2). The hydrogen desorption peaks arising from
7 silicon dihydride (α1) and silicon monohydride (α2) on the c-Si surface of the as-deposited
8 samples are observed. The α1 peak pressure of as-deposited heterocontacts with SiO_x interlayers
9 is lower than that of heterocontacts without a SiO_y interlayer. Furthermore, the hydrogen
10 desorption energies are found to be 1.76 and 2.13 eV for the TiO_x/c-Si and TiO_x/SC2-SiO_y/c-Si
11 heterocontacts, respectively. Therefore, the excellent passivation of the TiO_x/SC2-SiO_y/c-Si
12 heterocontacts is ascribed to the relatively high rupture energy of bonding between Si and H
13 atoms.

14

15 Keywords
16 surface passivation; silicon; titanium oxide; atomic layer deposition; hydrogen; thermal
17 desorption spectroscopy

18

1 1. Introduction

2 High-efficiency crystalline silicon (c-Si) solar cells are realized by implementation of carrier-
3 selective contacts (CSCs). CSCs can efficiently collect one type of photogenerated carrier in c-Si
4 at the terminals owing to good passivation at the c-Si surface and an appropriate work function
5 and band lineup for c-Si. The best type of CSC solar cell is Si heterojunction (SHJ) solar cells
6 employing stacks consisting of intrinsic hydrogenated amorphous Si (a-Si:H) and doped a-Si:H
7 on both the front and rear sides of c-Si [1–6]. The second-best type of solar cell uses tunnel oxide
8 passivated contacts (TOPCon) [7,8] or polycrystalline Si (pc-Si) on oxide (POLO) junctions
9 composed of stacks of doped pc-Si and ultrathin silicon oxide [9,10].

10 To obtain higher efficiency than high-efficiency solar cells such as SHJ, TOPCon, and POLO
11 junction solar cells, new CSC materials have been intensively studied. In general,
12 photogenerated carriers recombine in doped Si-based materials with high probability because of
13 enhanced Auger recombination (often termed parasitic absorption), which leads to a decrease in
14 the short-circuit current density (J_{SC}), and hence a reduction in the power conversion efficiency
15 [11–13]. In recent years, novel materials with a wider bandgap energy (E_g) have been studied to
16 increase J_{SC} by suppressing parasitic photon absorption. To date, transition metal oxides such as
17 molybdenum oxide [14-19], tungsten oxide [17-20], and vanadium oxide [17,18,21] have been
18 investigated as hole-selective contacts for CSC-based SHJ solar cells owing to their wider E_g and
19 high work function.

20 Titanium oxide prepared by atomic layer deposition (ALD) is a promising material for
21 electron-selective contacts for use in SHJ solar cells. The E_g value of a few-nanometer-thick
22 ALD-TiO_x layer is 3.3 eV [22,23], and thus the parasitic photon absorption is lower than those of

1 both a-Si:H (E_g = 1.7 eV) [11–13] and doped pc-Si (E_g = 1.12 eV) [24]. Although the electrical
2 and optical properties of TiO_x depend strongly on the composition x [25-27], near-stoichiometric
3 TiO_x can be formed by ALD [23,28]. Furthermore, a small conduction-band offset (<0.05 eV)
4 and large valence-band offset (>2.0 eV) are created at the ALD-TiO_x/c-Si interfaces, enhancing
5 carrier separation at the heterointerface [29,30]. Moreover, ALD is a self-limited film growth
6 method and has the advantages of precise thickness control, large-area uniformity, and little
7 deposition damage [31]. There are many reports that a thin ALD-TiO_x layer can provide a high
8 level of passivation of the c-Si surface after post-annealing [32-42]. Indeed, Yang *et al*.
9 successfully fabricated c-Si solar cells by employing a TiO_x/SiO_x stack and thus achieved a
10 conversion efficiency of 22.1% [43].

11 We previously reported that the improved passivation of the ALD-TiO_x/c-Si structure after
12 post-annealing originates mainly in desorption of hydrogen and hydrides such as water vapor
13 from the ALD-TiO_x/c-Si interface and subsequent formation of a silicon oxide (SiO_y) layer [41].
14 Furthermore, a substoichiometric SiO_y interlayer is formed by nitric acid (HNO_3) at room
15 temperature in the as-deposited state, and suggested that this SiO_y interlayer is key to obtaining
16 high-performance ALD-TiO_x/SiO_y stacks. This improvement in passivation is attributed mainly
17 to enhanced diffusion of oxygen and titanium atoms from ALD-TiO_x to SiO_y during post-
18 annealing [42]. Therefore, the use of a SiO_y interlayer with lower density to further enhance the
19 diffusion is expected to further improve the passivation of ALD- TiO_x. An ultrathin SiO_y layer
20 prepared by Standard Clean 2 (SC2, hydrochloric acid/hydrogen peroxide/deionized water =
21 1:1:4) at 60 °C (SC2-SiO_x hereafter) reportedly exhibits the lowest density in comparison with
22 other SiO_x layers formed by various wet chemical treatments [44,45].

In addition, hydrogen atoms are thought to positively affect passivation [1-6]. Although hydrogen atoms play an important role in inhibiting passivation of ALD-TiO_x/SiO_y stacks, their effects are not fully understood. Thermal desorption spectrometry (TDS) is widely used to investigate the effect of hydrogen atoms on the physical properties of metals [46,47], semiconductors [48,49], insulators [50,51], complex hydrides [52], and so on. Furthermore, the Si–H bonding energy can be derived from TDS analysis, which can reveal the relationship between passivation and the presence of hydrogen atoms.

In this study, we demonstrated that ALD-TiO_x deposited on the SC2-SiO_y interlayer can provide a high level of surface passivation on n-type c-Si. The compositional depth profiles of the heterojunctions were studied by high-resolution Rutherford backscattering (HR-RBS) and high-resolution elastic recoil detection analysis (HR-ERDA). The hydrogen desorption from the ALD-TiO_x/SiO_y/c-Si structures and its effects on the passivation were investigated using TDS.

2. Material and Methods

2.1. Sample preparation

All the ultrathin TiO_x layers were prepared by ALD (GEMStar-6, Arradiance) on both sides of double-side-polished, float-zone-grown n-type c-Si(100) substrates. The sample size, resistivity, and thickness were 3.0×3.0 cm^2, 2.0–5.0 Ω·cm, and approximately 280 µm, respectively. We fabricated the TiO_x/c-Si and the TiO_x/SiO_y/c-Si heterostructures. The n-c-Si substrates were dipped in 5% HF for 30 s to remove native oxides on the c-Si and hydrogen-passivated c-Si surfaces. To form SiO_y interlayers, some c-Si substrates were immersed in DIO_3 water at room

temperature for 10 min, and SC2 solution (35 w/v% hydrochloric acid/30 w/v% hydrogen peroxide/deionized water = 1:1:4) at 60 °C for 10 min. Then, the samples were deposited with symmetric TiO_x layers by ALD. The ALD-TiO_x layers were deposited at 150 °C using alternating cycles of tetrakis(dimethylamido)titanium and water vapor. The total thickness was set to 4 nm; the layer thickness of TiO_x was 4 nm for the TiO_x/c-Si heterocontacts and 3 nm for the TiO_x/SiO_y/c-Si heterocontacts. We performed forming gas annealing (FGA) at 350 °C for 3 min in a mixture of 97% Ar and 3% H_2 to enhance the surface passivation [41,42].

2.2. Characterization

The layer thickness was determined using a variable-angle spectroscopic ellipsometer (M-2000DI, J. A. Woollam). The Tauc–Lorentz model [53] was used to model the dielectric function of the ALD-TiO_x films, because transmission electron microscopy revealed that the ALD-TiO_x was in the amorphous phase [42]. The silicon oxide interlayer with a thickness of ~1 nm was taken into account in the optical model of the TiO_x/SiO_y/c-Si heterostructure. The mean square error (MSE) values of all the spectroscopic ellipsometry analyses were smaller than 2.0, indicating that the optical model is suitable for measuring the layer thickness.

To study the surface passivation performance of ALD-TiO_x on the c-Si surface, the injection-dependent effective lifetime (τ_{eff}) and the recombination current density (J_0) were measured before and after FGA using a WCT-120TS lifetime tester (Sinton Instrument) at room temperature [54,55].

To measure the contact resistivity (ρ_c), samples were prepared using the same procedure as that for the lifetime samples. After oxides on the rear side were removed by 5% HF treatment, 80-nm-thick antimony-doped gold was deposited on the rear side. Subsequently, six 80-nm-thick

aluminum dots with diameters of 0.2 to 1.0 mm were deposited on the TiO_x side by thermal evaporation through a metal mask defined using the Cox–Strack method. FGA was performed using the same process as that for the lifetime samples to activate the passivation effect and contact properties on the rear sides. We performed current versus voltage (*I*–*V*) measurements and obtained the contact resistivity from the relationship between the resistance and contact area. The details and examples of the Cox–Strack method are given elsewhere [56–58].

The contents of silicon, titanium, oxygen, carbon, hydrogen in the heterojunctions were measured by HR-RBS and HR-ERDA (HRBS500, KOBELCO). The details of HR-RBS and HR-ERDA is given elsewhere [59,60]. For HR-RBS measurements, a beam of 450 keV He^+ ion was produced by a 500 kV single-ended accelerator. The typical beam current was 30 nA. The samples were irradiated with the He^+ ion beam in ultra-high vacuum chamber. To utilize channeling technique [60,61], the incident angle of 45° was used (Si<110> channeling direction). The scattered He^+ ions from the samples at 55° were measured by a magnetic spectrometer. For HR-ERDA measurements, a collimated beam of 480 keV N^+ ion was used as primary beam (the incident angle was 70°). The typical beam current was about 0.2 nA. The recoiled H ions from the samples at 30° were measured by a magnetic spectrometer.

The hydrogen desorption from the TiO_x/c-Si and TiO_x/SiO_y/c-Si heterostructures was characterized by TDS using a quadrupole mass spectrometer as a hydrogen detector. The samples were heated to 800 °C at heating rates (HRs) of 200 to 600 °C/h. In the TDS measurements, the temperature and hydrogen partial pressure were recorded every 3 s. Before the samples were loaded in the chamber for TDS measurement, the H_2 partial pressure was measured before every measurement and used as a background value. In addition, background

1 spectra of the measured samples were acquired using the same temperature range and heating

2 range.

3

4 3. RESULTS AND DISCUSSION

5 Figure 1a-c shows the effective lifetime (τ_{eff}) of the TiO_x/n-c-Si, TiO_x/DIO_3-SiO_y/n-c-Si, and

6 TiO_x/SC2-SiO_y/n-c-Si heterocontacts as a function of excess minority carrier density (MCD).

7 Compared with TiO_x/n-c-Si heterocontacts, good passivation was obtained in the TiO_x/SC2-

8 SiO_y/n-c-Si heterocontacts before and after FGA, whereas the TiO_x/DIO_3-SiO_y/n-c-Si

9 heterocontacts exhibited almost identical effective lifetimes. The surface recombination velocity

10 (S_{surf}) of symmetrically coated c-Si is defined as follows,

11 $$\frac{1}{\tau_{eff}} = \frac{1}{\tau_{bulk}} + \frac{2S_{surf}}{W} \quad (1)$$

12 where, τ_{bulk} and W are lifetime of bulk Si and wafer thickness of 2.8×10^{-2} cm, respectively. The

13 τ_{bulk} is consisted of carrier lifetime determined by radiative recombination, Auger recombination

14 and Schochly-Read-Hall (SRH) recombination in bulk c-Si. The average τ_{eff} at an excess MCD

15 of 1.0×10^{15} cm^{-3} and calculated S_{surf} from the τ_{eff} values for the heterocontacts without SiO_y and

16 with DIO_3-SiO_y, and SC2-SiO_y, are summarized in Table 1. Here the τ_{bulk} is assumed to be

17 infinite in the calculation, since high-quality Si substrates were used. Hence, the actual values of

18 S_{surf} are slightly low in comparison with the calculated values of S_{surf}. The S_{surf} significantly

19 decreased by employing SC2-SiO_y interlayer. On the other hand, the S_{surf} for the TiO_x/DIO_3-

20 SiO_y/n-c-Si heterocontacts was same order of that for the TiO_x/n-c-Si heterocontacts. From these

21 results, the surface passivation is significantly improved by the SC2-SiO_y interlayer.

1 Recently, Sahasrabudhe *et al*. proposed that the formation of Si–O–Ti bonds at the TiO_x/c-Si
2 heterointerface is responsible for the outstanding performance of the heterojunction [37]. We
3 previously performed a comparative study of TiO_x/SiO_y/n-c-Si and TiO_x/n-c-Si heterocontacts
4 using high-resolution transmission electron microscopy and electron energy loss spectroscopy
5 [42]. In that paper, we remarked that the difference in the increase in τ_{eff} is due to the formation
6 of Si–O and/or Si–O–Ti bonds, which is caused by diffusion of Ti and O atoms from the ALD-
7 TiO_x layer into the SiO_y interlayer at low density [42]. The film density of SiO_y layers formed
8 using various chemicals was studied using glancing incidence X-ray reflectometry, and the SC2-
9 SiO_y layer showed the lowest density [44,45]. Therefore, we speculate that diffusion of Ti and O
10 atoms into the SC2-SiO_y interlayer is enhanced in the SC2-SiO_y interlayer with lower density,
11 and thus significant improvement of S_{surf} is realized. Silicon oxide is reportedly formed in
12 TiO_x/c-Si heterostructures after FGA [33,41]. On the other hand, it is reported that the DIO_3-SiO_y
13 exhibits relatively high film density [44,45]. The FGA-induced SiO_y/c-Si interface may be
14 defective in comparison with DIO_3-SiO_y/c-Si and thus the TiO_x/c-Si heterostructures showed
15 poor passivation effect among them. Although the DIO_3-SiO_y interlayer slightly improve
16 passivation effect, it may be enough dense to suppress diffusion of Ti atoms into the DIO_3-SiO_y
17 interlayer and the formation of Si–O–Ti bonds.

18 Figure 2a shows the *I*–*V* curves of the heterocontacts without SiO_y and with DIO_3-SiO_y, and
19 SC2-SiO_y after FGA. The *I-V* curves of the TiO_x/n-c-Si and TiO_x/DIO_3-SiO_y/n-c-Si
20 heterocontacts shows rectifying properties, while ohmic characteristic is observed for the
21 TiO_x/SC2-SiO_y/n-c-Si heterocontacts. To obtain values from the rectifying *I-V* curves, an
22 expanded Cox-Strack method is employed [62]. The total resistance (R_t) of a rectifying *I-V* curve

1 was determined from Cheng method and then the R_t value was utilized in Cox-Strack method.

2 The contact resistivity (ρ_c) values is calculated from the following equation,

3 $$R_t - R_s = \frac{\rho_c}{S} + R_0 \quad (2)$$

4 , where R_s is spreading resistance, S is contact area and R_0 is residual resistance. The details of

5 the expanded Cox-Strack method is given in [62].

6 Figure 2b show (R_t - R_s) as a function of S^{-1}. The ρ_c values of the heterocontacts are given in

7 Table 1. The TiO_x/SC2-SiO_y/n-c-Si heterocontacts exhibit the lowest ρ_c value. On the other hand,

8 ρ_c relatively large values were obtained in TiO_x/c-Si and TiO_x/DIO_3-SiO_y/n-c-Si heterocontacts.

9 In general, ρ_c depends on the resistivity of the materials themselves, the similarity of the Fermi

10 energy of Si and the work function of TiO_x, and the presence of defects at the heterointerfaces. It

11 is reported that the film density of SiO_y layers depend on chemicals [44,45]. The film density

12 would influence the resistivity of films and thus the *I-V* characteristics. Therefore, the obtained

13 ρ_c values are probably affected by compactness of SiO_y interlayer. In addition, the Fermi energy

14 of Si is known to be pinned at the defect level at the interfaces; thus, the contact resistance

15 become large. Hence, we consider that the low ρ_c value of the heterocontacts with SC2-SiO_y

16 interlayers can mainly be ascribed to the highly passivated interface, i.e., the lower interfacial

17 defect density, which is supported by the S_{surf} values in Table 1.

18 Figure 3a-f shows the elemental depth profiles of the TiO_x/n-c-Si, TiO_x/DIO_3-SiO_y/n-c-Si, and

19 TiO_x/SC2-SiO_y/n-c-Si heterocontacts before and after FGA. The dashed lines represent

20 channeling coefficient. For all samples, carbon concentration at surface became higher possibly

21 due to a carbon susceptor of the annealing furnace. The values of channeling coefficient are 100

in the TiO_x regions, indicating the TiO_x is amorphous structure before and after FGA. No significant difference in composition of TiO_x was observed for all samples. For as-deposited samples, the titanium and oxygen concentration are about 32-33 at% and 64 at% in the TiO_x regions, respectively. The Ti concentration were unchanged after FGA, while O concentration slightly increased up to about 65 at%. Furthermore, H contents in the TiO_x region decreased from about 5 to 2 at% after annealing. The larger H content in TiO_x layers before FGA possibly arose from hydroxyl groups in the oxide and the Ti precursor which contains many methyl groups. The smaller H content after FGA is the residual H species contained in the as-deposited samples and incorporated H atoms from forming gas. These results mean that hydrogen desorption at TiO_x layer was induced by FGA and thus near-stoichiometric TiO_x are formed after FGA, which is good agreement with the previous work [41,42].

As with the hydrogen in bulk TiO_x, hydrogen at around the heterointerfaces was reduced after FGA. For as-deposited state, hydrogen concentration of the TiO_x/c-Si heterointerface is higher than that of the TiO_x/DIO_3-SiO_y/c-Si and the TiO_x/SC2-SiO_y/c-Si heterointerfaces. The higher H concentration is resulted from H-terminated Si surface by HF treatments. The H-terminated surface is partly replaced as O-terminated surface owing to oxidizing treatment, which leads to low concentration of hydrogen at TiO_x/c-Si heterostructures with silicon oxide. To investigate hydrogen bonding states at the heterointerfaces, TDS measurements was carried out.

Figure 4 shows the TDS spectra of the TiO_x/SC2-SiO_y/c-Si heterocontacts before and after FGA. The dotted lines indicate the background. Two hydrogen effusion peaks at around 350 (α1) and 600 °C (α2) are observed for the as-deposited sample. The lower- and higher-temperature peaks represent the desorption from dihydrides and monohydrides, respectively [63–65]. A larger H_2 partial pressure is observed for the as-deposited sample. The large H content of

the sample before FGA is likely to originate in the Ti precursor, which contains many methyl groups. The decrease in H_2 pressure after FGA indicates that most of the hydrogen atoms in the sample are desorbed after FGA, which is consistent with H concentration in Fig. 3. Furthermore, we previously performed TDS measurements of TiO_x/c-Si heterocontacts and clarified that less hydrogen is incorporated into the TiO_x/c-Si heterocontacts after FGA [41]. Consequently, hydrogen atoms in the heterocontacts are desorbed after FGA, which suggests that the hydrogen atoms in the TiO_x/SiO_y/c-Si heterocontacts before FGA would play an important role in the improved passivation.

Figure 5a-c shows the TDS spectra of the TiO_x/c-Si, TiO_x/DIO_3-SiO_y/c-Si, and TiO_x/SC2-SiO_y/c-Si heterocontacts at heating rates (HRs) of 200, 300, 400, and 600 °C/h. The α1 and α2 peaks are observed in Figure 5a,c, whereas these peaks are weak in Figure 5b. The H_2 partial pressure became higher with increasing HR owing to an increase in the effusion rate of H_2 at high HRs. For the same effusion rate per unit temperature, the effusion rate increase with the HR. Hence, a higher HR results in a higher H_2 partial pressure. Note that FGA at 350 °C for 3 min was required to improve the passivation. The position of the α1 peak is close to the FGA temperature; thus, we focused on the α1 peaks in the TDS spectra. The α1 peak pressure of the TDS spectra obtained at an HR of 600 °C/h are 2.3×10^{-9}, 5.4×10^{-10}, and 1.8×10^{-9} Pa for the TiO_x/c-Si, TiO_x/DIO_3-SiO_y/c-Si, and TiO_x/SC2-SiO_y/c-Si heterocontacts, respectively. The lower α1 peak pressures of the TiO_x/DIO_3-SiO_y/c-Si and TiO_x/SC2-SiO_y/c-Si heterocontacts indicates a reduction in the number of Si–H2 bonds, which is probably attributable to presence of the SiO_y interlayer. In the as-deposited state, some of the Si–H2 bonds formed by HF treatment were replaced with Si–O bonds by oxidizing treatments. Furthermore, the film density of DIO_3-SiO_y is reportedly larger than that of SC2-SiO_y, indicating that a more compact SiO_y film is formed by

1 DIO_3 [44,45]. For the TiO_x/DIO_3-SiO_y/c-Si heterocontacts, a significant number of Si–H2 and
2 Si–H bonds were purged from the Si surface during oxidation, so they exhibited the lowest H_2
3 partial pressure.

4 In addition, the positions of the α1 and α2 peaks shifted to higher temperature with increasing
5 HR. The activation energy of H_2 desorption (E_{des}) can be calculated as

6 $$\ln\left(\frac{T_p^2}{HR}\right) = \frac{E_{des}}{k_B T_p} + \ln\left(\frac{E_{des}}{\sigma k_B}\right) \quad (3)$$

7 where T_p, k_B, and σ are the temperature of the peak, the Boltzmann constant, and the steric
8 factor, respectively [65-67]. E_{des} is determined from the slope of the plot of (T_p^2/HR) versus 1/T_p.
9 Figure 6 shows the dependence of ln(T_p^2/HR) on 1/T_p, where ln(T_p^2/HR) increases monotonically
10 with increasing 1/T_p. The τ_{eff}, ρ_c and E_{des} values are summarized in Table 1. The E_{des} values of
11 the TiO_x/DIO_3-SiO_y/c-Si heterocontacts cannot be obtained because the α1 peaks were not
12 observed at HRs of 200, 300, or 400 °C/h (as shown in Figure 5b). Stesmans reported that
13 activation energy of passivation of defects at SiO_2/c-Si interface with H atoms is about 1.5~1.6
14 eV [68, 69], indicating the extracted E_{des} values are reasonable order of magnitude. Further
15 studies are required to understand the elementary process from the absolute E_{des} values. The
16 TiO_x/SC2-SiO_y/c-Si heterostructures have a larger E_{des} value than the TiO_x/c-Si heterostructures,
17 suggesting that the dihydride on the c-Si surface is less likely to be desorbed during FGA.
18 Therefore, the excellent electrical properties of the TiO_x/SC2-SiO_y/c-Si heterocontacts results
19 from the difficulty of hydrogen desorption. Note that the diffusion of Ti and O atoms into the
20 SiO_y interlayer could be responsible for the enhanced passivation [37, 42]. It is worth noting that
21 RBS is impossible to distinguish between thin layer with high density and thick film with low

1 density, meaning Ti diffusion into SiO_x may happen during annealing. Therefore, the
2 improvement in the passivation can be explained by both the preservation of hydrogen atoms at
3 the c-Si surface and the diffusion of Ti and O atoms into the SiO_y interlayers. Identification of
4 the dominant mechanism is outside the scope of this study and is a subject for future research.
5
6 ## 4. CONCLUSION

7 We studied the effect of hydrogen desorption on the electrical properties of ALD-TiO_x on c-Si
8 with various SiO_x interlayers. The lowest S_{surf} of 9.6 cm/s and lowest ρ_c of 7.1 mΩ·cm^2 were
9 obtained using the SC2-SiO_y interlayer, indicating that the TiO_x/SC2-SiO_y/c-Si heterocontacts
10 exhibit good electrical properties. TDS measurements were performed to investigate hydrogen
11 desorption from the TiO_x/SiO_y/c-Si heterocontacts. The H_2 partial pressure decreased after FGA.
12 The α1 peak pressures of the TDS spectra at an HR of 600 °C/h were 2.3×10^{-9} Pa for the
13 TiO_x/c-Si heterocontact, 5.4×10^{-10} Pa for the TiO_x/DIO_3-SiO_y/c-Si heterocontact, and 1.8×10^{-9}
14 Pa for the TiO_x/SC2-SiO_y/c-Si heterocontact. The heterocontacts with a SiO_y interlayer had lower
15 H_2 partial pressures than the heterocontacts without SiO_y interlayers, because some of the Si–H2
16 bonds formed by hydrofluoric treatments were replaced with Si–O bonds by oxidation treatments.
17 The hydrogen desorption energy of the TiO_x/c-Si and TiO_x/SiO_y/c-Si heterocontacts are 1.76 and
18 2.13 eV, respectively. The excellent passivation by the SC2-SiO_y interlayer is attributed to a
19 higher rupture energy of Si–H2 bonding.
20

1 **Table 1.** Effective carrier lifetime at MCD of 1×10^{15} cm^{-3}, surface recombination velocity,
2 recombination current density, contact resistance, and activation energy of H_2 desorption from
3 the TiO_x/c-Si, TiO_x/DIO3-SiO_y/c-Si, and TiO_x/SC2-SiO_y/c-Si heterocontacts.

Structure	τ_{eff} at 1×10^{15} [ms][a)]	S_{surf} [cm/s][a)]	J_0 [fA·cm^{-2}][a)]	ρ_c [mΩ·cm^2][a)]	E_{des} [eV][b)]
TiO_x/c-Si	0.496	28.2	40.0	32.6	1.76
TiO_x/DIO_3-SiO_y/c-Si	0.596	23.5	71.2	20.9	-
TiO_x/SC2-SiO_y/c-Si	1.687	9.6	10.3	7.1	2.13

4 [a)]after FGA, [b)]before FGA
5

6

7 **Acknowledgements**
8 This work was supported by the New Energy and Industrial Technology Development
9 Organization (NEDO), MEXT; a Grant-in-Aid for Scientific Research on Innovative Areas
10 “Hydrogenomics” (JP18H05514); and the Inter-University Cooperative Research Program of the
11 Institute for Materials Research, Tohoku University (Proposal No. 18K0093). The authors thank
12 H. Miura and A. Shimizu for their technical help.

13

1

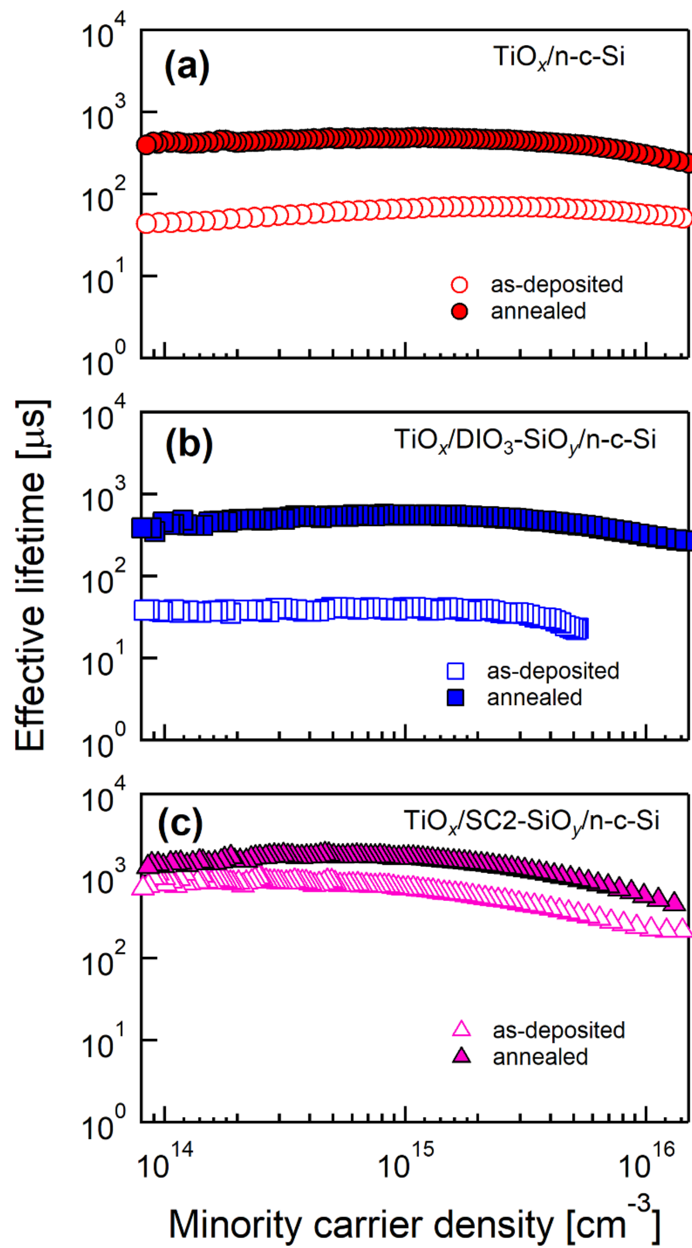

2 Fig. 1. Injection-dependent effective carrier lifetime of (a) TiO_x/n-c-Si, (b) TiO_x/DIO_3-SiO_y/n-c-

3 Si, and (c) TiO_x/SC2-SiO_y/n-c-Si heterocontacts before and after FGA.

4

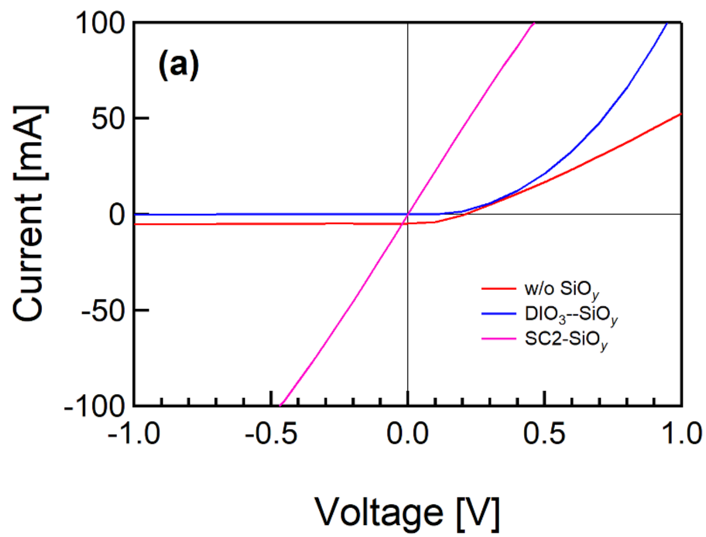

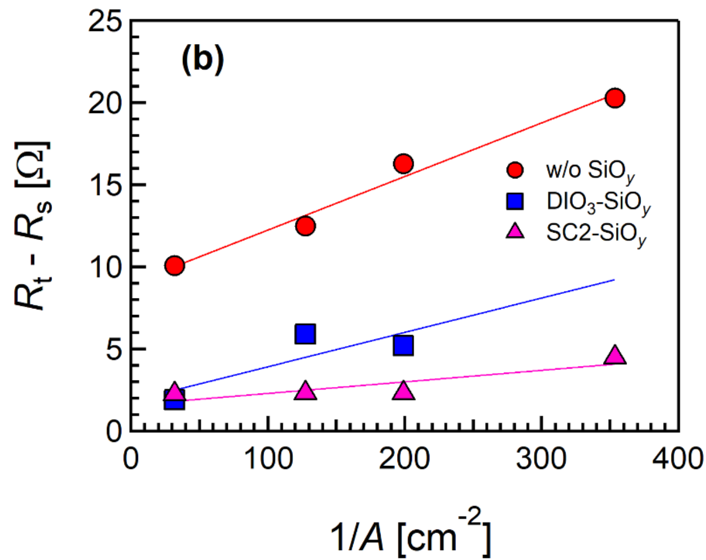

1

2 Fig. 2. (a) Current–voltage characteristics of the heterocontacts without SiO_y and with DIO_3-SiO_y,

3 and SC2-SiO_y after FGA. (b) Total resistance minus spreading resistance as a function of

4 reciprocal of contact area.

5

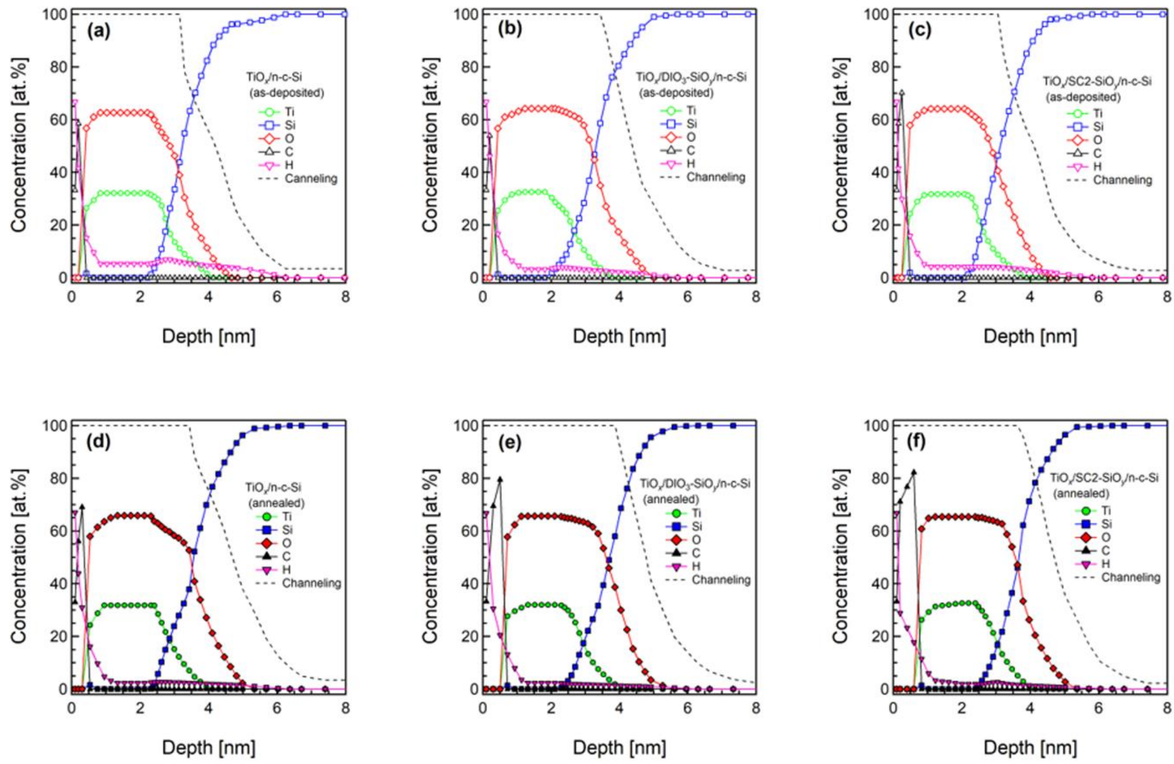

Fig. 3. Compositional depth profiles of (a, d) TiO_x/n-c-Si, (b, e) TiO_x/DIO_3-SiO_y/n-c-Si, and (c, f) TiO_x/SC2-SiO_y/n-c-Si heterocontacts before and after annealing at 350 ◦C for 3 min. The dotted lines represent channeling coefficient.

1

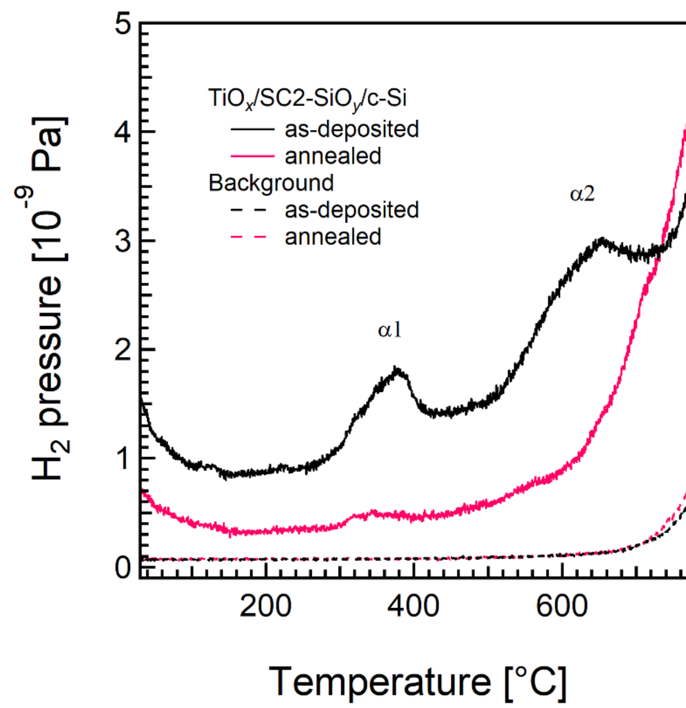

2 Fig. 4. TDS spectra of the TiO_x/SC2-SiO_y/c-Si heterostructures before and after FGA. The dotted

3 lines indicate the background spectra.

4

1

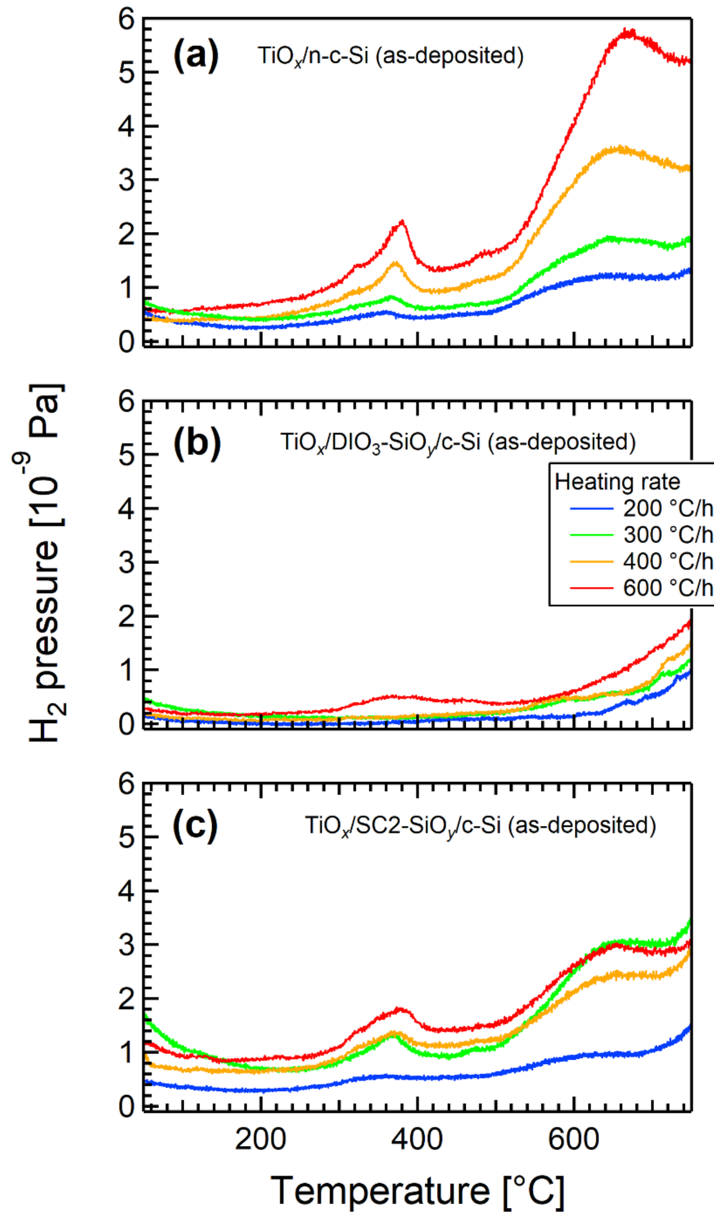

2 Fig. 5. TDS spectra of as-deposited TiO_x layers on n-c-Si (a) without a SiO_y/interlayer and 3 with

3 (b) DIO_3-SiO_y and (c) SC2-SiO_y interlayers. The heating rate is varied from 200 to 600 °C/h.

4

1

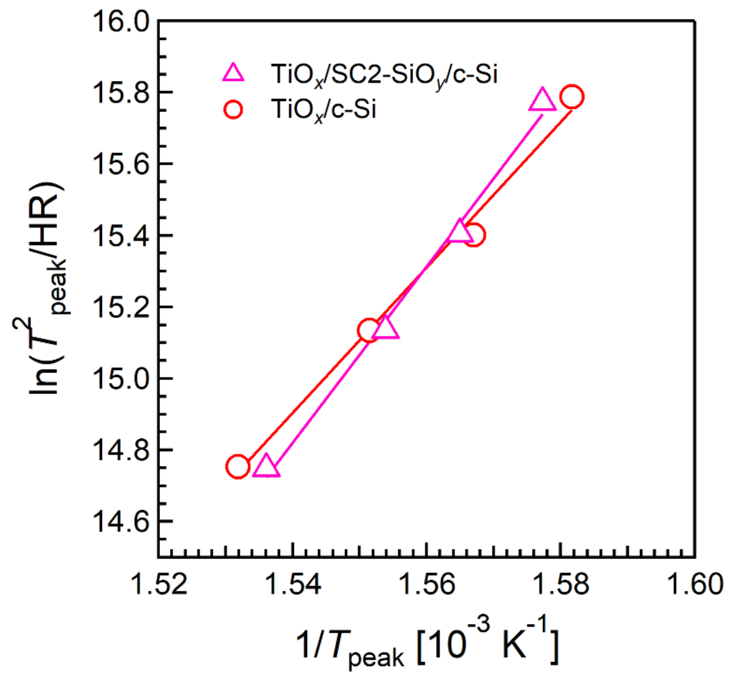

2 Fig. 6. $\ln(T_p^2/HR)$ vs. $1/T_p$ plots of the TiO_x/c-Si and TiO_x/SC2-SiO_y/c-Si heterocontacts.

3

1 **References**

2 [1] K. Masuko, M. Shigematsu, T. Hashiguchi, D. Fujishima, M. Kai, N. Yoshimura, T.
3 Yamaguchi, Y. Ichihashi, T. Mishima, N. Matsubara, T. Yamanishi, T. Takahama, M. Taguchi,
4 E. Maruyama, A. Okamoto, Achievement of More Than 25% Conversion Efficiency With
5 Crystalline Silicon Heterojunction Solar Cell, IEEE J. Photovoltaics 4 (2014), 1433-1435.

6 [2] M. Taguchi, A. Yano, S. Tohoda, K. Matsuyama, Y. Nakamura, T. Nishiwaki, K. Fujita,
7 and E. Maruyama, 24.7% Record Efficiency HIT Solar Cell on Thin Silicon Wafer, IEEE J.
8 Photovoltaics 4 (2014) 96-99.

9 [3] D. Adachi, J. L. Hernandez, K. Yamamoto, Impact of carrier recombination on fill factor
10 for large area heterojunction crystalline silicon solar cell with 25.1% efficiency, Appl. Phys. Lett.
11 107, 233506 (2015).

12 [4] K. Yoshikawa, H. Kawasaki, W. Yoshida, K. Konishi, K. Nakano, T. Uno, D. Adachi, M.
13 Kanematsu, H. Uzu, K. Yamamoto, Silicon heterojunction solar cell with interdigitated back
14 contacts for a photoconversion efficiency over 26%, Nat. Energy 2, 17032 (2017).

15 [5] C. Battaglia, A. Cuevas, S. De Wolf, High-efficiency crystalline silicon solar cells: status
16 and perspectives, Energy Environ. Sci. 9, (2016) 1552-1576.

17 [6] K. Gotoh, M. Wilde, S. Kato, S. Ogura, Y. Kurokawa, K. Fukutani, N. Usami, Hydrogen
18 concentration at a-Si:H/c-Si heterointerfaces—The impact of deposition temperature on
19 passivation performance, AIP Adv. 9, 075115 (2019).

1 [7] F. Feldmann, M. Bivour, C. Reichel, H. Steinkemper, M. Hermle, S. W. Glunz, Tunnel
2 oxide passivated contacts as an alternative to partial rear contacts, Sol. Energy Mater. Sol. Cells
3 131, (2014) 46-50.

4 [8] A. Richer, J. Benick, F. Feldmann, A. Fell, M. Hermle, S. W. Glunz, n-Type Si solar
5 cells with passivating electron contact: Identifying sources for efficiency limitations by wafer
6 thickness and resistivity variation, Sol. Energy Mater. Sol. Cells 173 (2017) 96-105.

7 [9] R. Peibst, U. Römer, Y. Larionova, M. Rienäcker, A. Merkle, N. Folchert, S. Reiter, M.
8 Turcu, B. Min, J. Krügener, D. Tetzlaff, E. Bugiel, T. Wietler, R. Brendel, Working principle of
9 carrier selective poly-Si/c-Si junctions: Is tunnelling the whole story?, Sol. Energy Mater. Sol.
10 Cells 158 (2016) 60-67.

11 [10] D. Tetzlaff, J. Krügener, Y. Larionova, S. Reiter, M. Turcu, F. Haase, R. Brendel, R.
12 Peibst, U. Höhne, J.-D. Kähler, T. F. Wietler, A simple method for pinhole detection in carrier
13 selective POLO-junctions for high efficiency silicon solar cells, Sol. Energy Mater. Sol. Cells
14 173 (2017) 106-110.

15 [11] A. A. Langford, M. L. Fleet, B. P. Nelson, Infrared absorption strength and hydrogen
16 content of hydrogenated amorphous silicon, Phys. Rev. B 45, 13367 (1992).

17 [12] A. S. Ferlauto, G. M. Ferreira, J. M. Pearce, C. R. Wronski, R. W. Collins, X. Deng, G.
18 Ganguly, Analytical model for the optical functions of amorphous semiconductors from the near-
19 infrared to ultraviolet: Applications in thin film photovoltaics, J. Appl. Phys. 92, 2424 (2002),.

1 [13] Z. C. Holman, A. Descoeudres, L. Barraud, F. Z. Fernandez, J. P. Seif, S. De Wolf, C.
2 Ballif, Current losses at the front of silicon heterojunction solar cells, IEEE J. Photovoltaics 2
3 (2012) 7-15.

4 [14] T. Kamioka, Y. Hayashi, Y. Isogai, K. Nakamura, Y. Ohshita, Effects of annealing
5 temperature on workfunction of MoO_x at MoO_x/SiO_2 interface and process-induced damage in
6 indium tin oxide/MoO_x/SiO_x/Si stack, Jpn. J. Appl. Phys. 57, 076501 (2018).

7 [15] C. Battaglia, S. M. de Nicolas, S. De Wolf, X. Yin, M. Zheng, C. Ballif, A. Javey, Silicon
8 heterojunction solar cell with passivated hole selective MoO_x contact, Appl. Phys. Lett. 104,
9 113902 (2014).

10 [16] J. Geissbuhler, J. Werner, S. M. Nicolas, L. Barraud, A. Hessler-Wyser, M. Despeisse, S.
11 Nicolay, A. Tomasi, B. Niesen, S. De Wolf, C. Ballif, 22.5% efficient silicon heterojunction
12 solar cell with molybdenum oxide hole collector, Appl. Phys. Lett. 107, 081601 (2015).

13 [17] L. G. Gerling, S. Mahato, A. Morales-Vilches, G. Masmitja, P. Ortega, C. Voz, R.
14 Alcubilla, J. Puigdollers, Transition metal oxides as hole-selective contacts in silicon
15 heterojunctions solar cells, Sol. Energy Mater. Sol. Cells 145 (2016) 109-115.

16 [18] L. G. Gerling, C. Voz, R. Alcubilla, J. Puigdollers, Origin of passivation in hole-selective
17 transition metal oxides for crystalline silicon heterojunction solar cells, J. Mater. Res. 32 (2016)
18 260-268.

19 [19] M. Bivour, J. Temmler, H. Steinkemper, M. Hermle, Molybdenum and tungsten oxide:
20 High work function wide band gap contact materials for hole selective contacts of silicon solar
21 cells, Sol. Energy Mater. Sol. Cells 142 (2015) 34-41.

1 [20] M. Mews, A. Lemaire, L. Korte, Sputtered Tungsten Oxide as Hole Contact for Silicon
2 Heterojunction Solar Cells, IEEE J. Photovoltaics 7 (2017) 1209-1215.

3 [21] G. Masmitjá, L. G. Gerling, P. Ortega, J. Puigdollers, I. Martin, C. Voz, R. Alcubilla,
4 V_2O_x-based hole-selective contacts for c-Si interdigitated back-contacted solar cells, J. Mater.
5 Chem. A 5 (2017) 9182-9189.

6 [22] J. Aarik, A. Aidla, A. Kiisler, T. Uustare, V. Sammelselg, Effect of crystal structure on
7 optical properties of TiO_2 films grown by atomic layer deposition, Thin Solid Films 305 (1997)
8 270-273.

9 [23] J. Bullock, Y. Wan, Z. Xu, S. Essig, M. Hettick, H. Wang, W. Ji, M. Boccard, A. Cuevas,
10 C. Ballif, A. Javey, Stable Dopant-Free Asymmetric Heterocontact Silicon Solar Cells with
11 Efficiencies above 20%, ACS Energy Lett. 3 (2018) 508-513.

12 [24] M. Rienacker, M. Bossmeyer, A. Merkle, U. Höhne, F. Haase, J. Krugener, R. Brendel, R.
13 Peibst, Junction Resistivity of Carrier-Selective Polysilicon on Oxide Junctions and Its Impact on
14 Solar Cell Performance, IEEE J. Photovoltaics 7 (2017) 11-18.

15 [25] J. Xu, D. Wang, H. Yao, K. Bu, J. Pan, J. He, F. Xu, Z. Hong, X. Chen, F. Huang, Nano
16 Titanium Monoxide Crystals and Unusual Superconductivity at 11 K, Adv. Mater. 30, 1706240
17 (2018).

18 [26] W.-C. Peng, Y.-C. Chen, J.-L. Ou, S.-L. Ou, R.-H. Horng, D.-S. Wuu, Tunability of p-
19 and n-channel TiO_x thin film transistors, Sci. Rep. 8, 9255 (2018).

1 [27] A. D. Inglis, Y. L. Page, P. Strobel, C. M. Hurd, Electrical conductance of crystalline
2 TinO2n-1 for n=4-9, J. Phys. C: Solid State Phys. 16 (1983) 317-333.

3 [28] V. Naumann, M. Otto, R. B. Wehrspohn, M. Werner, C. Hagendorf, Interface and
4 material characterization of thin ALD-Al_2O_3 layers on crystalline silicon, Energy Procedia 27,
5 (2012) 312-318.

6 [29] S. Avasthi, W. E. McClain, G. Man, A. Kahn, J. Schwar, J. C. Strum, Hole-blocking
7 titanium-oxide/silicon heterojunction and its application to photovoltaics, Appl. Phys, Lett. 102,
8 203901 (2013).

9 [30] K. A. Nagamatsu, S. Avasthi, G. Sahasrabudhe, G. Man, J. Jhaveri, A. H. Berg, J.
10 Schwartz, A. Kahn, S. Wagner, J. C. Strum, Titanium dioxide/silicon hole-blocking selective
11 contact to enable double-heterojunction crystalline silicon-based solar cell, Appl. Phys. Lett. 106,
12 123906 (2015).

13 [31] R. L. Puurunen, Surface chemistry of atomic layer deposition: A case study for the
14 trimethylaluminum/water process, J. Appl. Phys. 97, 121301 (2005).

15 [32] X. Yang, P. Zheng, Q. Bi, K. Weber, Silicon heterojunction solar cells with electron
16 selective TiO_x contact, Sol. Energy Mater. Sol. Cells 150 (2016) 32-38.

17 [33] X. Yang, Q. Bi, H. Ali, K. Davis, W. V. Schoenfeld, K. Weber, High-Performance TiO_2-
18 Based Electron-Selective Contacts for Crystalline Silicon Solar Cells, Adv. Mater. 28 (2016)
19 5891-5897.

1 [34] R. Brendel and R. Peidst, Contact selectivity and efficiency in crystalline silicon
2 photovoltaics, IEEE J. Photovoltaics 6, (2016) 1413-1420.

3 [35] B. Liao, B. Hoex, A. G. Aberle, D. Chi, C. S. Bhatia, Excellent c-Si surface passivation
4 by low-temperature atomic layer deposited titanium oxide, Appl. Phys. Lett. 104, 253903 (2014).

5 [36] B. Liao, B. Hoex, K. D. Shetty, P. K. Basu, C. S. Bhatia, Passivation of Boron-Doped
6 Industrial Silicon Emitters by Thermal Atomic Layer Deposited Titanium Oxide, IEEE J.
7 Photovoltaics 5 (2015) 1062-1066.

8 [37] G. Sahasrabudhe, S. M. Rupich, J. Jhaveri, A. H. Berg, K. A. Nagamatsu, G. Man, Y. J.
9 Chabal, A. Kahn, S. Wagner, J. C. Strum, J. Schwartz, Low-Temperature Synthesis of a TiO_2/Si
10 Heterojunction, J. Am. Chem. Soc. 137 (2015) 14842-14845.

11 [38] K. M. Gad, D. Vossing, A. Richter, B. Rayner, L. M. Reindl, S. E. Mohney, M.
12 Kasemann, Ultrathin Titanium Dioxide Nanolayers by Atomic Layer Deposition for Surface
13 Passivation of Crystalline Silicon, IEEE J. Photovoltaics 6 (2016) 649-653.

14 [39] M. M. Plakhotnyuk, N. Schuler, E. Shkodin, R. A. Vijayan, S. Masilamani, M.
15 Varadharajaperumal, A. Crovetto, O. Hansen, Surface passivation and carrier selectivity of the
16 thermal-atomic-layer-deposited TiO_2 on crystalline silicon, Jpn. J. Appl. Phys. 56, 08MA18
17 (2017).

18 [40] V. Titova, B. Veith-Wolf, D. Startsev, J. Schmidt, Effective passivation of crystalline
19 silicon surfaces by ultrathin atomic-layer-deposited TiO_x layers, Energy Procedia 124, (2017)
20 441-447.

1 [41] T. Mochizuki, K. Gotoh, A. Ohta, S. Ogura, Y. Kurokawa, S. Miyazaki, K. Fukutani, N.
2 Usami, Activation mechanism of TiO_x passivating layer on crystalline Si, Appl. Phys. Express 11,
3 102301 (2018).

4 [42] T. Mochizuki, K. Gotoh, Y. Kurokawa, T. Yamamoto, N. Usami, Local Structure of High
5 Performance TiO_x Electron-Selective Contact Revealed by Electron Energy Loss Spectroscopy,
6 Adv. Mater. Interfaces 6, 1801645 (2018).

7 [43] X. Yang, K. Weber, Z. Hameiri, S. D. Wolf, Industrially feasible, dopant-free, carrier-
8 selective contacts for high-efficiency silicon solar cells, Prog. Photovoltaics Res. Appl. 25 (2017)
9 896-904.

10 [44] N. Awaji, Y. Sugita, S. Ohkubo, T. Nakanishi, K. Takasaki, S. Komiya, High-Accuracy
11 X-ray Reflectivity Study of Native Oxide Formed in Chemical Treatment, Jpn. J. Appl. Phys. 34
12 (1995) L1013-L1016.

13 [45] Y. Sugita, S. Watanabe, N. Awaji, X-Ray Reflectometry and Infrared Analysis of Native
14 Oxides on Si (100) Formed by Chemical Treatment, Jpn. J. Appl. Phys. 31 (1996) 5437-5443.

15 [46] M. Wang, E. Akiyama, K. Tsuzaki, Hydrogen degradation of a boron-bearing steel with
16 1050 and 1300 MPa strength levels, Scr. Mater. 52 (2005) 403-408.

17 [47] T. Chida, Y. Hagihara, E. Akiyama, K. Iwagana, S. Takagi, M. Hayakawa, H. Ohishi, D.
18 Hirakami, T. Tarui, Comparison of Constant Load, SSRT and CSRT Methods for Hydrogen
19 Embrittlement Evaluation Using Round Bar Specimens of High Strength Steels, ISIJ Int. 56
20 (2016) 1268-1275.

1 [48] K. Nakada, S. Miyajima, M. Konagai, Amorphous silicon oxide passivation films for
2 silicon heterojunction solar cells studied by hydrogen evolution, Jpn. J. Appl. Phys. 53, 04ER13
3 (2014).

4 [49] W. Beyer, Hydrogen effusion: a probe for surface desorption and diffusion, Physica B
5 170 (1991) 105-114.

6 [50] D. Cheng, K. Tsukamoto, H. Komiyama, Y. Nishimoto, N. Tokumasu, K. Maeda,
7 Thermal desorption spectra of SiO_2 films deposited on Si and on thermal SiO_2 by
8 tetraethylorthosilicate/O_3 atmospheric-pressure chemical vapor deposition, J. Appl. Phys. 85,
9 (1999) 7140-7145.

10 [51] K. Murase, N. Yabumoto, Y. Komine, Thermal Desorption Studies of Silicon Dioxide
11 Deposited by Atmospheric - Pressure Chemical Vapor Deposition Using Tetraethylorthosilicate
12 and Ozone, J. Electrochem. Soc. 140 (1993) 1722-1727.

13 [52] S. Orimo, Y. Nakamori, J. R. Eliseo, A. Züttel, C. M. Jenson, Complex Hydrides for
14 Hydrogen Storage, Chem. Rev. 107 (2007) 4111-4132.

15 [53] G. E. Jellison Jr., F. A. Modine, Parameterization of the optical functions of amorphous
16 materials in the interband region, Appl. Phys. Lett. 69 (1996) 371-373.

17 [54] A. Cuevas, R. A. Sinton, Prediction of the open-circuit voltage of solar cells from the
18 steady-state photoconductance, Prog. Photovoltaics Res. Appl. 5 (1997) 79-90.

1 [55] R. A. Sinton, A. Cuevas, Contactless determination of current-voltage characteristics and
2 minority-carrier lifetimes in semiconductors from quasi-steady-state photoconductance data,
3 Appl. Phys. Lett. 69 (1996) 2510-2512.

4 [56] R. Cox, H. Strack, Ohmic contacts for GaAs devices, Solid-State Electron. 10 (1967)
5 1213-1218.

6 [57] K. Gotoh, T. Mochizuki, Y. Kurokawa, N. Usami, Tuning the Electrical Properties of
7 Titanium Oxide Bilayers Prepared by Atomic Layer Deposition at Different Temperatures, Phys.
8 Status Solidi A 216, 1900495 (2019).

9 [58] R. P. Gupta, J. B. White, O. D. Iyore, U. Chakrabarti, H. N. Alshareef, B. E. Gnade,
10 Determination of Contact Resistivity by the Cox and Strack Method for Metal Contacts to Bulk
11 Bismuth Antimony Telluride, Electrochem. Solid-State Lett. 12 (2009) H302-H304.

12 [59] B. Brijs, T. Sajavaara, S. Giangrandi, T. Janssens, T. Conard, K. Arstila, K. Nakajima, K.
13 Kimura, A. Bergmaier, G. Dollinger, A. Vantomme, W. Vandervorst, The analysis of a thin
14 $SiO_2/Si_3N_4/SiO_2$ stack: A comparative study of low-energy heavy ion elastic recoil detection.
15 high-resolution Rutherford backscattering and ion mass spectroscopy, Nucl. Instrum. Method
16 Phys. Res. B 249 (2006) 847-850.

17 [60] L.J. van Ijzendoorn, High energy scattering and recoil spectrometry in applied materials
18 science, Anal. Chim. Acta 297 (1994) 55-72.

19 [61] P. Malar, T. K. Chan, C.S. Ho, T. Osipowicz, HRBS/channeling studies of ultra-thin ITO
20 films on Si, Nucl. Instrum. Method Phys. Res. B 266 (2008) 1464-1467.

[62] W. Wang, H. Lin, Z. Yang, Z. Wang, J. Wang, L. Zhang, M. Liao, Y. Zeng, P. Gao, B. Yan, J. Ye, An expanded Cox and Strack method for precise extraction of specific contact resistance of transition metal oxide/n-silicon heterojunction, IEEE Photovolt. 9 (2019) 1113-1120.

[63] S. De Wolf, C. Ballif, M. Kondo, Kinetics of a-Si:H bulk defect and a-Si:H/c-Si interface-state reduction, Phys. Rev. B 85, 113302 (2012).

[64] P. A. Taylor, R. M. Wallace, C. C. Cheng, W. H. Weinberg, M. J. Dresser, W. J. Choyke, J. T. Yates Jr., Adsorption and decomposition of acetylene on silicon(100)-(2×1), J. Am. Chem. Soc. 114 (1992) 6754-6760.

[65] P. Martín, J. F. Fernández, C. R. Sánchez, TDS Applied to Investigate the Hydrogen and Silane Desorption from Porous Silicon, Phys. Status Solidi A 182 (2000) 255-260.

[66] W. Y. Choo, J. Y. Lee, Thermal analysis of trapped hydrogen in pure iron, Metall. Trans. A 13 (1982) 135-140.

[67] H. Lüth, Solid Surfaces, Interfaces and Thin Films, sixth ed., Springer, Berlin, 2015.

[68] A. Stesmans, Influence of interface relaxation on passivation kinetics in H_2 of coordination P_b defects at the (111)Si/SiO_2 interface revealed by electron spin resonance, J. Appl. Phys. 92 (2002) 1317.

[69] A. Stesmans, Passivation of P_{b0} and P_{b1} interface defects in thermal (100) Si/SiO_2 with molecular hydrogen, Appl. Phys. Lett. 68 (1996) 2076.